On the Use of Dual Co-Polarized Radar Data to Derive a Sea Surface Doppler Model—Part 2: Simulation and Validation

Shengren Fan, Biao Zhang, *Senior Member, IEEE*, Artem Moiseev, Vladimir Kudryavtsev, Johnny A. Johannessen, and Bertrand Chapron

Abstract— The Doppler shift obtained from synthetic aperture radar (SAR) measurements comprises the combined contribution to the radial motion of the ocean surface induced by the sea state (wind waves and swell) and underlying surface currents. Hence, to obtain reliable estimates of the ocean surface current (OCS), the sea-state-induced Doppler shifts must be accurately estimated and eliminated. In this study, we use a semiempirical dual co-polarization Doppler velocity (DPDop) model, presented in the companion paper, to calculate sea-state-induced Doppler shifts using buoy-measured wind speed, wind direction, and ocean wave spectra. The DPDop model-simulated Doppler shifts are compared with the collocated Sentinel-1B SAR Wave (WV) mode observations at the 24° and 37° incidence angles, showing a bias of −0.24 Hz and a root-mean-square error (RMSE) of 5.55 Hz. This evaluation is also implemented on a simplified DPDop model at the same incidence angles. The model inputs include wind fields from the European Center for Medium-Range Weather Forecasts (ECMWF) and wave characteristic parameters (e.g.,

significant wave height (SWH), mean wave direction, and mean wavenumber) from WAVEWATCH III (WW3). The estimated Doppler shifts are validated using the ascending and descending observations of Sentinel-1B WV over the global ocean. Furthermore, the comparisons show that the bias and RMSE are −0.71 and 9.25 Hz, respectively. Based on accurate wave bias correction, we obtain the radial current speeds of the ocean surface from the Doppler shift measurements. The estimated current speeds are compared with the collocated high-frequency (HF) radar measurements, with a bias of −0.04 m/s and an RMSE of 0.15 m/s. These results suggest that the original and simplified DPDop models can be used to estimate sea-state-induced Doppler shifts and, thus, derive accurate surface current retrievals.

I. Introduction

THE ocean surface roughness sensed by spaceborne synthetic aperture radars (SARs) is linked to surface wind, waves, and currents, as well as surfactants. Previous studies have demonstrated that ocean surface current (OSC) information can be obtained from SAR Doppler shift measurements [1], [2], [3], [4], [5], [6], [7], [8]. The SAR-measured instantaneous Doppler shift comprises various contributions from surface wind, waves, and currents. Therefore, accurately estimating and eliminating the sea-state-induced Doppler shift signal is crucial for deriving reliable OSCs.

The sea-state-induced Doppler shifts include contributions from wind waves and the swell. The Doppler shift associated with wind waves has been investigated under different wind conditions and radar configurations (i.e., incidence angle, radar look angle, frequencies, and polarization) [9], [10], [11], [12], [13], [14]. Among them, an empirical geophysical model function, CDOP, was developed to predict the wind-wave-induced Doppler shift at VV and HH polarizations [9]. However, CDOP only considered the contribution of wind waves to the Doppler shift, while that of swell was ignored. Recently, another empirical model, CDOP3S, has been developed to estimate wind-wave- and swell-induced Doppler shifts using the triple collocation of Sentinel-1B SAR Wave (WV) mode observations, wind fields from ECMWF, and wave fields from WW3 [7]. Compared to CDOP, CDOP3S yields significant improvements because the additional effect of swell on Doppler shift was considered. However, CDOP3S cannot reproduce realistic sea-state-induced contributions to Doppler

Shengren Fan is with the School of Marine Sciences, Nanjing University of Information Science and Technology, Nanjing 210044, China (e-mail: sr_fan@nuist.edu.cn).

Biao Zhang is with the School of Marine Sciences, Nanjing University of Information Science and Technology, Nanjing 210044, China, also with the Southern Marine Science and Engineering Guangdong Laboratory (Zhuhai), Zhuhai 51900, China, and also with the Fisheries and Oceans Canada, Bedford Institute of Oceanography, Dartmouth, NS B2Y 4A2, Canada (e-mail: zhangbiao@nuist.edu.cn).

Artem Moiseev is with the Nansen Environmental and Remote Sensing Center, 5007 Bergen, Norway (e-mail: Artem.Moiseev@nersc.no).

Vladimir Kudryavtsev is with the Satellite Oceanography Laboratory, Russian State Hydrometeorological University, 195196 St. Petersburg, Russia, and also with Marine Hydrophysical Institute RAS, 299011 Sebastopol, Russia (e-mail: kudr@rshu.ru).

Johnny A. Johannessen is with the Nansen Environmental and Remote Sensing Center, 5007 Bergen, Norway, and also with the Geophysical Institute, University of Bergen, 5006 Bergen, Norway (e-mail: Johnny. Johannessen@nersc.no).

Bertrand Chapron is with the Laboratoire d'Océanographie Physique et Spatiale, IFREMER, 29280 Plouzané, France (e-mail: Bertrand.Chapron@ ifremer.fr).

Digital Object Identifier 10.1109/TGRS.2023.3246771

shift observations due to the overfitting of the model during training. Thus, an updated model, CDOP3SX, was proposed to compute Doppler shifts using the range-directed component of the wind vector and wave orbital velocity [8]. CDOP3SX yields more realistic Doppler shifts than CDOP and CDOP3S because it considers the combined wind- and wave-induced motion. Based on the CDOP3SX model, the estimates of the sea state contribution under mixed wind fetch conditions were improved from a refined empirical model (CDOP3SiX) [8] by separating the contributions of wind waves and swell to Doppler shift observations.

Unlike the aforementioned empirical models, a semiempirical ocean surface Doppler velocity model (DPDop; see [15], a companion paper) was developed to estimate Doppler shifts associated with wind waves and swell. The dual co-polarization Doppler velocity (DPDop) model was derived from the geophysical model function C-SARMOD2 [16] and the empirical wave-breaking scattering model [17]. The DPDop model can be used to estimate wave-induced Doppler shifts, given the wind speed, wind direction, and ocean wave spectra. Compared with the empirical models, the DPDop model can simulate each component of Doppler velocity, such as the velocities of the resonant Bragg waves and breaking waves, the contributions of tilt and hydrodynamic modulations of scattering facets by the long surface waves. However, the performance of the DPDop model has not yet been substantially evaluated. Moreover, wave spectra are sometimes unavailable, which impedes the application of the DPDop model.

In this study, we first simplify the original DPDop model to extend its usability. The simplified DPDop model can be applied to estimate wave-induced Doppler shifts using wave characteristic parameters (e.g., significant wave height (SWH) and mean wave direction, etc.) instead of surface wave spectra. Subsequently, the wave-induced Doppler shifts simulated by the original and simplified DPDop models are systematically validated with the collocated Sentinel-1B SAR WV mode observations. Finally, we retrieve the radial current speeds of the ocean surface from Sentinel-1B WV data and compare them with high-frequency (HF) radar measurements. The remainder of this article is organized as follows. Section II describes the data set. In Section III, we present the simulation and validation results of the original and simplified DPDop models. The conclusion is given in Section IV.

II. DATASET

A. Sentinel-1 Data

In this study, Sentinel-1B Level 2 ocean surface radial velocity (RVL) data are used to validate the original and simplified DPDop models. The RVL data are derived from 78 190 SAR global WV scenes from December 2017 to January 2018 [see Fig. 1(a) and (b)]. The WV mode alternately acquires data in 20×20 km vignettes with a 5×5 m spatial resolution every 100 km along the orbit, with two different incidence angles (24° for WV1 and 37° for WV2). In addition to RVL, the Sentinel-1B Level 2 data contain auxiliary information, including the collocated wind and wave fields from ECMWF and WW3, respectively.
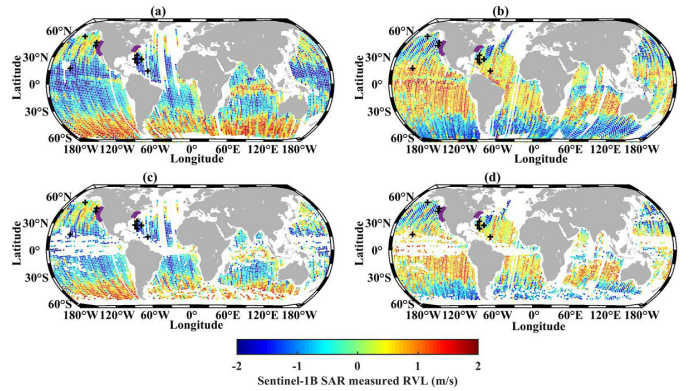

Fig. 1. Radial Doppler velocities of the global ocean surface derived from Sentinel-1B WV mode observations from December 2017 to January 2018: (a) ascending and (b) descending. (c) and (d) are similar to (a) and (b), but observations acquired over regions with moderate and strong currents are discarded. The black pluses denote the location of the NDBC buoys. The purple areas on (a)–(d) represent the regions of the HF radar surface current measurements.

To obtain an accurate RVL, the Doppler shift due to the relative velocity of the SAR and rotating earth (f_{dc}^{geo}) and the Doppler shift induced by an antenna electronic mis-pointing (f_{dc}^{elec}) need to be estimated and subtracted from the SAR-measured Doppler shift. The details for estimating these two nongeophysical Doppler terms can be found in [7] and [18]. The geophysical Doppler shift (f_{dc}^{phys}) induced by ocean surface wind, waves, and currents can be further derived according to $f_{dc}^{phys} = f_{dc} - f_{dc}^{geo} - f_{dc}^{elec}$. In turn, ocean surface RVLs are estimated using the geophysical Doppler shift

$$U_{rvl} = -\frac{\pi f_{dc}^{phys}}{k_e \sin\theta} \tag{1}$$

where k_e is the electromagnetic wavenumber (for the C-band, $k_e = 112$ rad/m), and θ is the radar incidence angle. Note that U_{rvl} is positive or negative when the target on the ocean surface moves away from or toward the radar, respectively. It should be noted that the RVL depends on wind-wave-induced motion. The wind waves are generated by both meridional and zonal wind components. The same sign of RVL in the entire 30°S ~ 30°N belt indicates that the zonal wind is dominant. The meridional wind, with different signs in northeasterly and southeasterly trade wind zones, is less important. As shown in Fig. 1, the zonal wind moves toward and away from the radar for ascending and descending tracks, thereby yielding the RVL with opposite signs.

Notably, Sentinel-1B RVL includes contributions from waves and currents, while Doppler velocity simulations from the original and simplified DPDop models are only associated with wave-induced motion. Previous studies have shown that small-scale ocean currents significantly affect the sea state [19], [20]. To compare the simulated and measured Doppler shifts, we need to remove the contributions of currents to the Sentinel-1B RVL measurements. Thus, Sentinel-1B WV observations acquired over regions where near-surface currents are larger than 0.15 m/s are removed using the drifter-derived climatology of global near-surface ocean currents [21]. We also exclude WV scenes acquired over relatively shallow

water areas (<1000 m) and regions close to land (<110 km) to alleviate the effect of ocean bottom topography on surface waves [22] and coastal wind fields. Moreover, to avoid the effects of sea ice, WV acquisitions over high latitudes (>55°) are discarded. Based on the above criterion, 34 333 WV observations are removed, but there are still 43 857 data pairs [see Fig. 1(c) and (d)] that can be used for the model validation.

B. HF Radar Data

HF radars are shore-based microwave instruments and can measure OSCs over a large region (~300 km) of the coastal ocean under most weather conditions. The HF radar transmits electromagnetic waves of 3–50 MHz (10–100 m wavelengths), which travel along the ocean surface beyond the horizon and are scattered from the surface waves of half radar wavelength. The Doppler shift of the backscattered signal is used to measure the radial current speed of the ocean surface [23]. The accuracies of the HF radar current measurements typically range from 5 to 20 cm/s [24], [25], [26]. In this study, we use hourly HF radar current measurements with a spatial resolution of 6 km to validate SAR-derived radial current speeds. These data are acquired in the east and west coastal areas of the USA and can be accessed on the HF Radar Network (HFRNet) website[1].

C. Buoy Data

Sentinel-1B Level 2 RVL data were collocated with nine in situ National Data Buoy Center (NDBC) buoys. The buoy locations are shown in Fig. 1. These buoys measure hourly wind speed and direction, as well as characteristic wave parameters, such as SWH and dominant wave periods, which are available on the NDBC website[2]. The buoy measurements and RVL data were required to be within a spatial distance of 50 km and a time interval of 30 min. The buoy-measured wind speeds are converted to the 10 m height using a logarithmical wind profile equation [27].

Moreover, these buoys also measure the directional wave spectrum $S(f, \varphi)$, which can be estimated using the nondirectional wave height spectrum $C_{11}(f)$ and the directional spreading function $D(f, \varphi)$: $S(f, \varphi) = C_{11}(f) \times D(f, \varphi)$. Note that the original directional spreading function $D^o(f, \varphi)$ cannot be directly used to calculate the directional wave spectrum because it is broad. Thus, we use the maximum entropy method [28] to estimate the new directional spreading function $D^N(f, \varphi)$. The details of the $D^N(f, \varphi)$ estimates are presented in Appendix. The directional frequency spectrum can be determined by the following equation:

$$S(f, \varphi) = C_{11}(f)D^N(f, \varphi) \tag{2}$$

where f is the wave frequency and φ is the wave direction (oceanographic convention). The directional wavenumber spectrum $S(k, \varphi)$ is given as follows:

$$S(k, \varphi) = S(f, \varphi)\frac{df}{dk} = \frac{S(f, \varphi)}{8\pi^2 f}\left[\tanh(kh)+\frac{kh}{\cosh^2(kh)}\right] \tag{3}$$

[1]https://hfrnet-tds.ucsd.edu/thredds/catalog.html
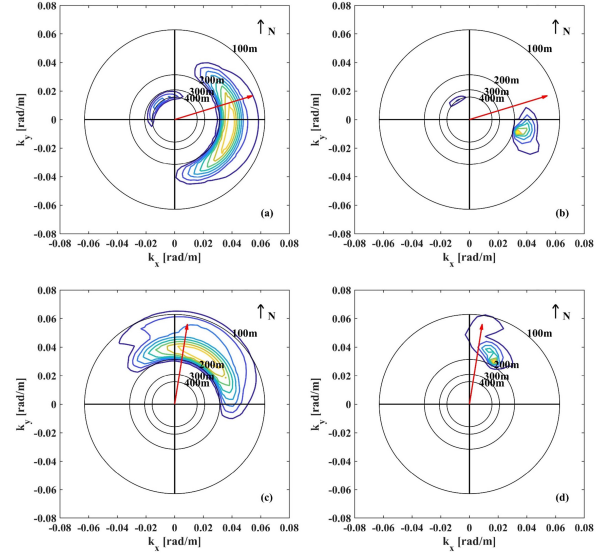[2]https://www.ndbc.noaa.gov

Fig. 2. (a) and (b) are the estimated ocean wave spectra of the mixed sea state (wind wave and swell) with the original and new directional spreading functions. The red arrows represent the wind direction. (c) and (d) are similar to (a) and (b), except for the pure wind wave.

where k is the wavenumber and h is the finite water depth. Subsequently, the omnidirectional elevation spectrum $S(k)$ is obtained as follows:

$$S(k) = \int_{-\pi}^{\pi} S(k, \varphi)d\varphi. \tag{4}$$

Consequently, the omnidirectional saturation spectrum is given by the following equation:

$$B(k) = k^3 S(k). \tag{5}$$

Based on (2) and (3), we calculate the wave spectra using the original and new directional spreading functions. Fig. 2 shows the wave spectra estimates for two typical cases. The first case represents the mixed sea state conditions comprising two different wave systems (a swell and a wind wave), while the second is a pure wind wave. For both cases, the estimated wave spectra using the new directional spreading function are narrower than those with the original one. In order to compare the original DPDop model simulations with Sentinel-1B observations, Sentinel-1B WV data were collocated with NDBC buoy wind and wave observations. A total number of 30 matchup pairs were obtained, including Doppler shift, RVL, wind speed and direction, and ocean wave spectra. Fig. 3 illustrates the estimated ocean wave spectra consisting of the different wave systems (wind waves, mixed sea state, and swell). These wave spectra are calculated using a buoy-measured nondirectional wave height spectrum and the new directional spreading function, which are used to calculate wave-induced Doppler shifts using the original DPDop model.

III. MODEL SIMULATIONS AND VALIDATION

A. Validation of the Original DPDop Model

Regarding the data set mentioned in Section II, the Sentinel-1B data acquired over regions with moderate and strong ocean currents have been filtered, and thus, the Doppler
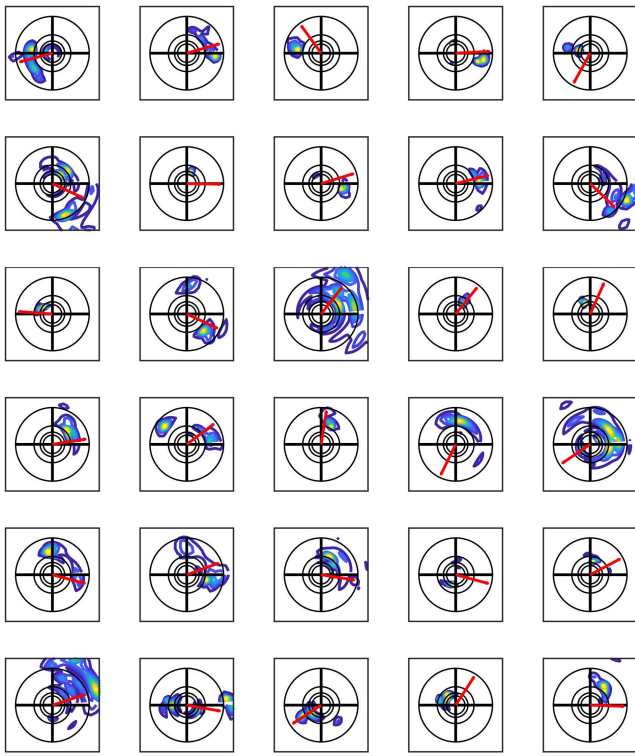
Fig. 3. Estimated ocean wave spectra (e.g., wind waves, mixed sea state, and swell) using the buoy-measured nondirectional wave height spectrum and the new directional spreading function. The abscissa and ordinate and contour values of this figure are same as in Fig. 2. The red arrows represent the wind direction.
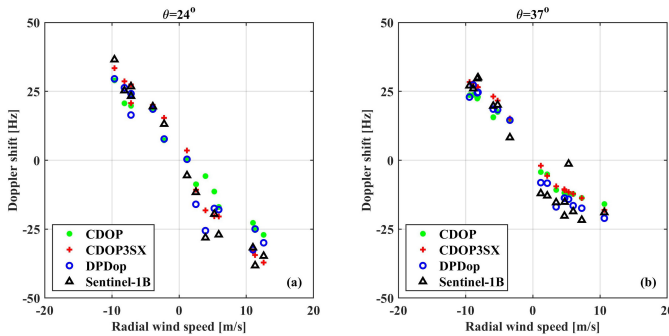

Fig. 4. Dependence of the simulated and measured Doppler shifts at the (a) 24° and (b) 37° incidence angles on the radial wind speed. The solid green circles, red pluses, blue open circles, and black triangles represent the simulations from the CDOP, CDOP3SX, and DPDop models and Sentinel-1B observations, respectively. Note that the simulated and observed Doppler shifts are induced by wind waves and swell.

shift and RVL measurements can be considered as a combined contribution of wind waves and swell. Based on this rationale, the original DPDop model can be evaluated using Sentinel-1B Doppler shift measurements. Fig. 4 illustrates how the measured and simulated Doppler shifts increase with an increase in radial wind speeds, whether the wind comes toward or moves away from the radar. The simulated Doppler shifts from various empirical or semiempirical models, such as CDOP, CDOP3SX, and DPDop, are overall in agreement with Sentinel-1B observations at the 24° and 37° incidence angles. The differences between CDOP simulations and Sentinel-1B measurements may be because CDOP does not consider the
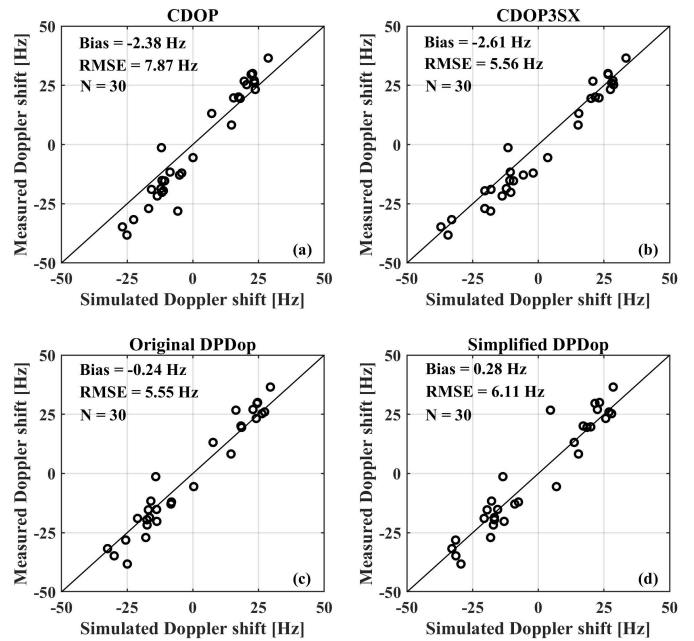

Fig. 5. Comparisons of the simulated Doppler shifts to the Sentinel-1B observations. (a) CDOP, (b) CDOP3SX, (c) original DPDop, and (d) simplified DPDop models. Note that the simulated and observed Doppler shifts are induced by wind waves and swell.

contribution of swell to the Doppler shift. We also observed that CDOP3SX simulations are significantly smaller than Sentinel-1B observations at the 37° incidence angle when the wind moves away from the radar. The underestimations are possibly associated with the fact that CDOP3SX cannot well simulate wave-induced Doppler shifts for underdeveloped seas in the coastal zone [8]. Compared to CDOP and CDOP3SX, DPDop-simulated Doppler shifts are closer to Sentinel-1B measurements. This is because the DPDop model development does not require the observed Doppler shift and, thus, the residual nongeophysical signals associated with calibration errors are not involved.

The simulated and measured Doppler shifts were quantitatively compared. Fig. 5(a) shows that the CDOP simulations exhibit discrepancies with Sentinel-1B observations, with a large bias of -2.38 Hz and an RMSE of 7.87 Hz. The CDOP model ignores the contribution of swell to the Doppler shift, which accounts for the distinct differences. CDOP3SX seems to improve Doppler shift simulations in terms of a reduced RMSE of 5.56 Hz [see Fig. 5(b)]. However, compared to the measured Doppler shifts, the increased negative bias (-2.61 Hz) indicates that CDOP3SX simulations are underestimated. Fig. 5(c) illustrates that the DPDop-simulated Doppler shifts are consistent with the Sentinel-1B measurements; moreover, the bias and RMSE are -0.24 and 5.55 Hz, respectively. These errors are much smaller than those of CDOP because DPDop considers the mixed contributions of swell and wind waves to the Doppler shift. We also compare the simulated Doppler shifts from the simplified DPDop model with those measured by Sentinel-1B. Fig. 5(d) shows that the bias (0.28 Hz) and RMSE (6.11 Hz) of the simplified DPDop model are comparable to those of the original DPDop model.

The details of the simplified DPDop model are introduced in Section III-B.

B. Simplified DPDop Model

According to the companion paper [15], the governing equation of the DPDop model is as follows:

$$V_D = u_s + (1-P_{NP})c_B + P_{NP}c_{NP} + c^T + P_{NP}c_{wb}^H \quad (6)$$

where V_D is the ocean surface RVL due to the combined wind-wave-, swell-, and current-induced motion. u_s is the OSC velocity; c_B and c_{NP} are the Doppler velocities of the Bragg scattering and breaking wave facets; c^T represents the tilting effect of the scattering facets (Bragg waves and breakers) by longer surface waves (see (9), (12), (19), and (29) in the companion paper); and c_{wb}^H represents the effect of hydrodynamic modulations of wave breaking by longer surface waves. The term P_{NP} is the key parameter of the original DPDop model and represents the relative contribution of nonpolarized scattering to the total radar backscattering (see Figs. 2–4 in the companion paper). Accordingly, $(1 - P_{NP})$ is the relative contribution of Bragg scattering.

The ocean surface wave spectra are the key input parameter of the original DPDop model. However, only a few wave rider buoys can provide wave spectra observations. The sparse wave spectra measurements over the global ocean limit the substantial validations and applications of this model. Although microwave satellites, such as SAR and wave scatterometer, can measure wave spectra from space, their accuracy needs to be improved, especially under high wind conditions. As introduced in the companion paper, c^T and c_{wb}^H in (6) are functions of the wave spectra and the main contribution to c^T and c_{wb}^H comes from the longest surface waves. Therefore, the integral parameters of dominant waves (e.g., SWH, mean wave direction, and mean wavenumber) can be used as DPDop input for calculating Doppler velocity, when wave spectra observations are not available.

In the simplified DPDop model, we do not distinguish different wave systems, such as the wind waves and swell (or even the number of swell systems), in the mixed sea state. Instead, we propose to handle a "single" wave system consisting of large-scale waves existing in real sea states for the purpose of simplification. Thus, wave characteristic parameters can be derived from directional wavenumber spectrum $S(k, \varphi)$ or the omnidirectional elevation spectrum $S(k)$. The wave energy (E) is calculated by the following equation:

$$E = \int_0^{k_l} S(k)dk \quad (7)$$

where k_l is the buoy-measured maximum wavenumber. Furthermore, the SWH is estimated from the wave energy

$$H_s = 4\sqrt{E}. \quad (8)$$

The mean wavenumber is defined as follows:

$$k_m = \frac{\int_0^{k_l} S(k)kdk}{\int_0^{k_l} S(k)dk}. \quad (9)$$

TABLE I
SUMMARY OF THE WAVE CHARACTERISTIC PARAMETERS DERIVED FROM THE WAVEDIRECTIONAL SPECTRA ESTIMATED WITH THE NEW DIRECTIONAL SPREADINGFUNCTION. THE TWO TYPICAL CASES (I AND II) CORRESPOND TO A MIXED SEASTATE (WIND WAVE AND SWELL) AND A PURE WIND WAVE, RESPECTIVELY

Case ID	H_s(m)	k_m(rad/m)	φ_m(deg)
I	3.44	7.83×10^{-2}	92.98
II	3.71	8.11×10^{-2}	22.89

Furthermore, the mean wave direction can be calculated from the directional wavenumber spectrum $S(k, \varphi)$

$$\cos(\varphi_m) = \frac{\iint \cos(\varphi)S(k,\varphi)dkd\varphi}{\iint S(k,\varphi)dkd\varphi}$$

$$\sin(\varphi_m) = \frac{\iint \sin(\varphi)S(k,\varphi)dkd\varphi}{\iint S(k,\varphi)dkd\varphi}$$

$$\varphi_m = \arctan\left[\frac{\sin(\varphi_m)}{\cos(\varphi_m)}\right]. \quad (10)$$

Table I summarizes the wave characteristic parameters derived from the wave directional spectra [ocean wave spectra in Fig. 2(b) and (d)] estimated with the new directional spreading function. These parameters are key input components of the simplified DPDop model.

The surface saturation spectrum is simplified by the following equation:

$$B(k, \varphi) = k^3 E\delta(k - k_m)\delta(\varphi - \varphi_m). \quad (11)$$

Here, E is the wave energy linked to the SWH through (8). k_m and φ_m are the mean wavenumber and mean wave direction, respectively, defined by (9) and (10). $\delta(x)$ is the Dirac delta function. For simplification, we substitute (11) in (20) and (29) in the companion paper [15]. These two equations describe the contributions of tilt modulations of Bragg waves and breakers and the hydrodynamic modulations of wave breaking by long surface waves to Doppler velocity, respectively.

$$c^T = -\cot\theta M_f^t \cos(\varphi_R - \varphi_m)C_m k_m^2 E \quad (12)$$

and

$$c_{wb}^H = \left[\cos(\varphi_R\varphi_m)M_{1wb}^h(\varphi_m, k_m) + \cot\theta M_{2wb}^h(\varphi_m, k_m)\right]C_m k_m^2 E. \quad (13)$$

Here, φ_R is the radar look direction, θ is the radar incidence angle, k_m is the mean wavenumber, and $C_m = C(k_m)$ is the phase velocity at the mean wavenumber. The tilt and hydrodynamic modulation transfer functions (M_f^t and M_{wb}^h) are defined in the companion paper (see [15, eqs. (18) and (27)]).

Based on (12) and (13), we estimate the last four terms in (6). The sum of these terms represents the wave-induced Doppler velocity. Subsequently, the estimated Doppler velocity is converted to the Doppler shift using (1). In turn, the wind-wave- and swell-induced contributions to the Doppler shift can be expressed as a function of the radar geometry, wind speed and direction, and wave characteristic parameters

$$f_D = DPDop(u_{10}, \varphi_w, H_s, \varphi_m, k_m, \theta, \varphi_R, \text{pol}). \quad (14)$$
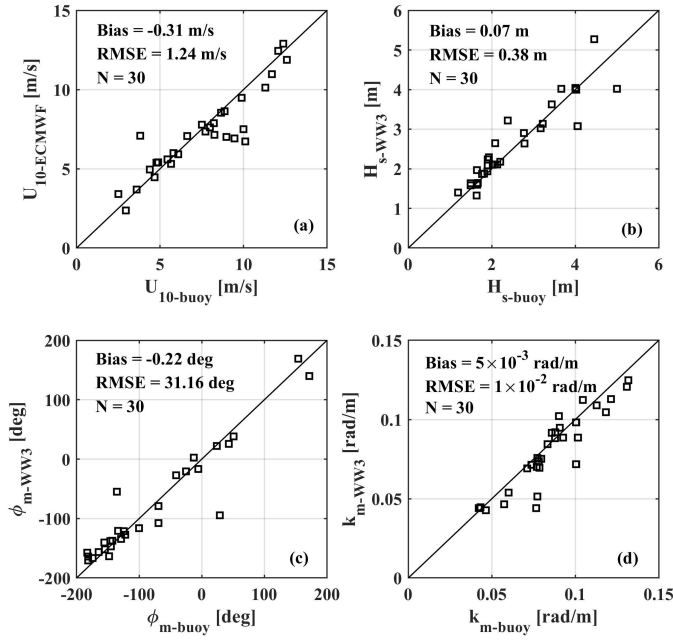
Fig. 6. Comparisons between the ECMWF wind and WW3 wave data and the buoy observations. (a) Wind speed, (b) SWH, (c) mean wave direction, and (d) mean wavenumber.
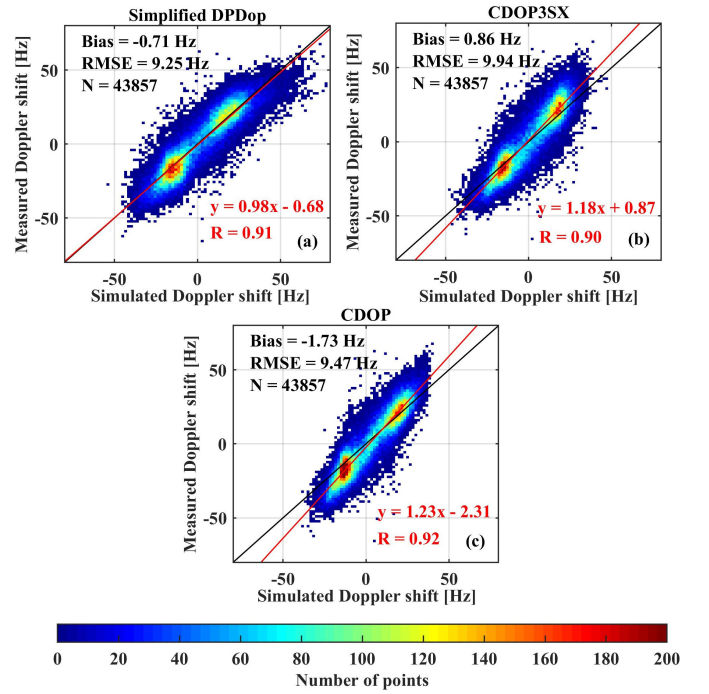

Fig. 7. Comparisons of the simulated Doppler shifts with the Sentinel-1B observations. (a) Simplified DPDop model, (b) CDOP3SX, and (c) CDOP. The red lines in (a)–(c) represent the linear regression between the measured and simulated Doppler shifts. The color bar represents the number of observations. Note that the simulated and observed Doppler shifts are induced by wind waves and swell.

Here, f_D is the Doppler shift, u_{10} is the ocean surface wind speed at 10 m height, φ_w is the wind direction, H_s is the SWH, φ_m is the mean wave direction, k_m is the mean wavenumber, θ is the incidence angle, and φ_R is the radar look direction. Additionally, pol stands for the polarization option (HH or VV). The (14) represents the simplified DPDop model.

C. Validation of the Simplified DPDop Model

The inputs of the simplified DPDop model are the wind fields and the wave characteristic parameters. Thus, we can use the collocated wind and wave data from ECMWF and WW3 to estimate the wave-induced Doppler shift and compare it with Sentinel-1B observations. Before the comparison, we assess the wind and wave data from ECMWF and WW3 using the collocated buoy observations. Fig. 6(a) shows that the ECMWF wind speeds are in good agreement with the buoy observations when wind speeds range from 0 to 15 m/s. The bias and RMSE are −0.31 and 1.24 m/s, respectively. We also observed small deviations between the WW3 SWHs and buoy measurements, with a bias of 0.07 m and an RMSE of 0.38 m [see Fig. 6(b)]. The range of SWH for the comparison is between 1 and 6 m. Moreover, the mean wave direction and mean wavenumber from WW3 are comparable to the buoy data except for individual outliers, as shown in Fig. 6(c) and (d).

Fig. 7(a) illustrates the comparisons between the simulated Doppler shifts from the simplified DPDop model and the ascending and descending WV observations of Sentinel-1B over the global ocean. The bias and RMSE are −0.71 and 9.25 Hz, respectively. We implemented similar evaluations on CDOP3SX and CDOP, and the results are shown in Fig. 7(b) and (c). The bias and RMSE of CDOP3SX are slightly larger than those of the simplified DPDop model.

CDOP has a similar RMSE value to CDOP3SX and the simplified DPDop model; however, it has a superior negative bias of −1.73 Hz. In addition to the bias and RMSE, we also estimate the standard deviation (std) of three models. The std is 9.22 Hz for the simplified DPDop model. The corresponding values are 9.90 and 9.31 Hz for CDOP3SX and CDOP, respectively. Compared to the Sentinel-1B observations, CDOP underestimates the Doppler shifts by 23%. In the collocated dataset, the maximum wind speed from ECMWF is 25.29 m/s, and this high wind speed corresponds to a freak wave with an SWH of 8.53 m from WW3. Under these wind and wave conditions, the Sentinel-1B measured Doppler shift is −41.77 Hz, indicating that a high sea state can induce large Doppler shifts. According to (12) and (13), large wave energy produces considerable tilt and hydrodynamic modulations of scattering facets by long surface waves. These two modulations contribute significantly to the measured Doppler shift. The simplified DPDop-simulated Doppler shift is −40.89 Hz, consistent with Sentinel-1B observations. This suggests that the simplified DPDop model can reproduce a realistic wave-induced Doppler shift, at least for this case. In contrast, the CDOP and CDOP3SX estimates deviate from the Sentinel-1B measurements, with simulated Doppler shifts of −32.20 and −34.88 Hz, respectively.

In order to retrieve ocean surface radial current speed, the contributions of wind waves and swell to the Doppler shift need to be eliminated. To this end, we first use the simplified DPDop model to estimate wave-induced Doppler shifts, with given wind fields from ECMWF and wave characteristic
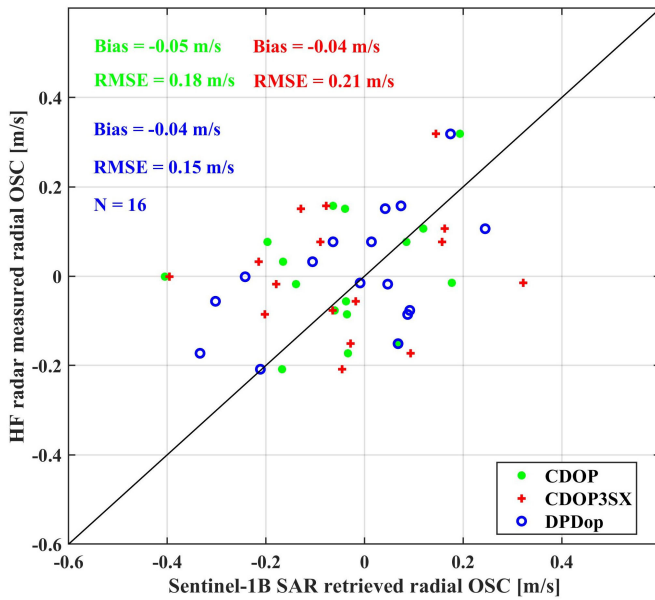
Fig. 8. Comparison of the Sentinel-1B SAR-retrieved radial OSC based on the various wave bias correction models with the collocated HF radar measurements. The solid green circles, red pluses, and blue open circles represent the CDOP, CDOP3SX, and DPDop models, respectively.

parameters from WW3. Subsequently, Doppler shifts arising from surface currents are derived from the differences between Sentinel-1B measurements and the simplified DPDop model estimates. Finally, radial current speeds are easily obtained according to (1). We compare the retrieved radial current speeds and the collocated HF radar observations, as shown in Fig. 8. The Sentinel-1B SAR WV images and HF radar measurements must be within a spatial interval of 10 km and a time interval of 60 min. Based on this matchup criterion; 16 collocation pairs are obtained to validate the current speed. The comparison of the retrieved radial current speeds with the HF radar observations demonstrates consistency regarding the small bias and RMSE values. The bias and RMSE are -0.04 and 0.15 m/s for the simplified DPDop model, -0.05 and 0.18 m/s for CDOP, and -0.04 and 0.21 m/s for CDOP3SX, respectively. These errors are related to inaccurate estimates of Doppler shifts associated with the nongeophysical terms and sea state, as well as the uncertainty of the HF radar measurements. The nongeophysical terms include the Doppler shift arising from the relative velocity of the satellite and rotating earth and the Doppler shift induced by an antenna electronic mis-pointing. These nongeophysical terms must be precisely estimated and eliminated from the measured Doppler shift. However, the geometric Doppler shift is difficult to calculate accurately from the satellite attitude and orbit parameters. Thus, SAR images with land coverage help to derive reliable corrections of bias induced by geometry and antenna electronic mis-pointing. Moreover, sea-state-induced Doppler shifts should also be accurately calculated to obtain reasonable ocean surface radial current retrievals. This can be conducted using the original and simplified DPDop models because they both consider the contributions of wind waves and swell to the Doppler shift.

IV. CONCLUSION

The SAR-measured geophysical Doppler shifts from the ocean surface comprise various contributions from wind waves, swell, and currents. To derive reliable OSC information from SAR observations, wave-induced Doppler shifts must be precisely estimated and eliminated. Thus, a semiempirical model, termed the original DPDop, has been developed to calculate Doppler shifts associated with wind waves and swell [15]. However, this model has not yet been comprehensively evaluated. In this study, we use the original DPDop model to simulate wave-induced Doppler shifts using buoy wind and wave spectra data and compare them with the collocated Sentinel-1B SAR WV mode observations. The bias and RMSE are -0.24 and 5.55 Hz, respectively.

A key input of the original DPDop model is the surface wave spectra, which are not always available over the global ocean. Thus, we simplify the original DPDop model to extend its application range. The inputs of the simplified DPDop model are wind speed and direction, SWH, mean wave direction, and mean wavenumber, rather than wave spectra. We use the wind fields from ECMWF and wave characteristic parameters from WW3 to calculate the wave-induced Doppler shifts. The estimates are compared with the ascending and descending Doppler shift measurements of the Sentinel-1B SAR WV mode over the global ocean, showing a bias of -0.71 Hz and an RMSE of 9.25 Hz. We also use the buoy-measured wind and wave parameters to compute wind wave and swell-induced Doppler shifts and compare them to the collocated Sentinel-1B observations. The bias and RMSE are 0.28 and 6.11 Hz. Moreover, the simplified DPDop model simulations are compared to the CDOP and CDOP3SX estimates. We observed that DPDop is comparable to CDOP3SX but outperforms CDOP. This is likely because the swell contribution to the Doppler shift was ignored in CDOP. In contrast, the DPDop and CDOP3SX models consider contributions from wind waves and swell.

The radial current speeds of the ocean surface are retrieved from Sentinel-1B SAR WV mode Doppler shift observations and compared with coastal HF radar measurements. The bias between the SAR and HF radar observations is -0.04 m/s, and the RMSE is 0.15 m/s. This suggests that the DPDop model can reliably estimate the sea-state-induced Doppler shift and, consequently, obtain accurate OSC information. Further current validations are required using additional in situ observations from surface drifters and numerical simulations from the regional ocean circulation model.

APPENDIX A

The new directional spreading function is defined as follows:

$$D^N(f, \varphi) = \frac{1 - p_1 \bar{c}_1 - p_2 \bar{c}_2}{|1 - p_1 e_1 - p_2 e_2|^2}. \tag{15}$$

Here, $\bar{c}_1$ represents the conjugate of c_1, and the parameters of c_1, c_2, p_1, p_2, e_1, and e_2 are written as follows:

$$c_1 = a_1 + i b_1, \quad c_2 = a_2 + i b_2 \tag{16}$$

$$p_1 = \frac{c_1 - c_2 \bar{c}_1}{1 - |c_1|^2}, \quad p_2 = c_2 - c_1 p_1 \qquad (17)$$

$$e_1 = \cos(\alpha) - i\sin(\alpha), \quad e_2 = \cos(2\alpha) - i\sin(2\alpha). \qquad (18)$$

The range of α is $0 - 2\pi$, and the parameters of a_1, a_2, b_1, b_2 are given as follows:

$$a_1 = \cos(\alpha_1) \times \frac{r_1}{100}, \quad a_2 = \cos(2\alpha_2) \times \frac{r_2}{100} \qquad (19)$$

$$b_1 = \sin(\alpha_1) \times \frac{r_1}{100}, \quad b_2 = \sin(2\alpha_2) \times \frac{r_2}{100}. \qquad (20)$$

Here, r_1 and r_2 are the first and second normalized polar coordinates of the nondimensional Fourier coefficients, respectively; α_1 and α_2 are the mean and principal wave directions, respectively.

REFERENCES

[1] R. Romeiser and D. R. Thompson, "Numerical study on the along-track interferometric radar imaging mechanism of oceanic surface currents," *IEEE Trans. Geosci. Remote Sens.*, vol. 38, no. 1, pp. 446–458, Jan. 2000.

[2] B. Chapron, "Direct measurements of ocean surface velocity from space: Interpretation and validation," *J. Geophys. Res.*, vol. 110, no. 7, pp. 1–17, 2005.

[3] J. A. Johannessen et al., "Direct ocean surface velocity measurements from space: Improved quantitative interpretation of ENVISAT ASAR observations," *Geophys. Res. Lett.*, vol. 35, no. 22, pp. 1–6, 2008.

[4] M. Krug, A. Mouche, F. Collard, J. A. Johannessen, and B. Chapron, "Mapping the Agulhas current from space: An assessment of ASAR surface current velocities," *J. Geophys. Res., Oceans*, vol. 115, no. 10, pp. 1–14, Oct. 2010.

[5] M. W. Hansen, F. Collard, K. Dagestad, J. A. Johannessen, P. Fabry, and B. Chapron, "Retrieval of sea surface range velocities from Envisat ASAR Doppler centroid measurements," *IEEE Trans. Geosci. Remote Sens.*, vol. 49, no. 10, pp. 3582–3592, Oct. 2011.

[6] A. Moiseev, H. Johnsen, M. W. Hansen, and J. A. Johannessen, "Evaluation of radial ocean surface currents derived from Sentinel-1 IW Doppler shift using coastal radar and Lagrangian surface drifter observations," *J. Geophys. Res., Oceans*, vol. 125, no. 4, Apr. 2020, Art. no. e2019JC015743.

[7] A. Moiseev, H. Johnsen, J. A. Johannessen, F. Collard, and G. Guitton, "On removal of sea state contribution to Sentinel-1 Doppler shift for retrieving reliable ocean surface current," *J. Geophys. Res., Oceans*, vol. 125, no. 9, Sep. 2020, Art. no. e2020JC016288.

[8] A. Moiseev, J. A. Johannessen, and H. Johnsen, "Towards retrieving reliable ocean surface currents in the coastal zone from the Sentinel-1 Doppler shift observations," *J. Geophys. Res., Oceans*, vol. 127, no. 5, May 2022, Art. no. e2021JC018201.

[9] A. A. Mouche et al., "On the use of Doppler shift for sea surface wind retrieval from SAR," *IEEE Trans. Geosci. Remote Sens.*, vol. 50, no. 7, pp. 2901–2909, Jul. 2012.

[10] A. C. H. Martin, C. Gommenginger, J. Marquez, S. Doody, V. Navarro, and C. Buck, "Wind-wave-induced velocity in ATI SAR ocean surface currents: First experimental evidence from an airborne campaign," *J. Geophys. Res., Oceans*, vol. 121, no. 3, pp. 1640–1653, Mar. 2016.

[11] Y. Y. Yurovsky, V. N. Kudryavtsev, S. A. Grodsky, and B. Chapron, "Ka-band dual copolarized empirical model for the sea surface radar cross section," *IEEE Trans. Geosci. Remote Sens.*, vol. 55, no. 3, pp. 1629–1647, Mar. 2017.

[12] Y. Yurovsky, V. Kudryavtsev, S. Grodsky, and B. Chapron, "Sea surface Ka-band Doppler measurements: Analysis and model development," *Remote Sens.*, vol. 11, no. 7, p. 839, Apr. 2019.

[13] Y. Y. Yurovsky, V. N. Kudryavtsev, B. Chapron, and S. A. Grodsky, "Modulation of Ka-band Doppler radar signals backscattered from the sea surface," *IEEE Trans. Geosci. Remote Sens.*, vol. 56, no. 5, pp. 2931–2948, May 2018.

[14] A. Elyouncha, L. E. B. Eriksson, R. Romeiser, and L. M. H. Ulander, "Empirical relationship between the Doppler centroid derived from X-band spaceborne InSAR data and wind vectors," *IEEE Trans. Geosci. Remote Sens.*, vol. 60, 2022, Art. no. 4201120.

[15] V. Kudryavtsev, S. Fan, B. Zhang, B. Chapron, J. A. Johannessen, and A. Moiseev, "On the use of dual co-polarized radar data to derive a sea surface Doppler model—Part 1: Approach," *IEEE Trans. Geosci. Remote Sens.*, vol. 61, 2023, Art. no. 4201013.

[16] Y. Lu, B. Zhang, W. Perrie, A. A. Mouche, X. Li, and H. Wang, "A C-band geophysical model function for determining coastal wind speed using synthetic aperture radar," *IEEE J. Sel. Topics Appl. Earth Observ. Remote Sens.*, vol. 11, no. 7, pp. 2417–2428, Jul. 2018.

[17] V. N. Kudryavtsev, S. Fan, B. Zhang, A. A. Mouche, and B. Chapron, "On quad-polarized SAR measurements of the ocean surface," *IEEE Trans. Geosci. Remote Sens.*, vol. 57, no. 11, pp. 8362–8370, Nov. 2019.

[18] A. C. H. Martin, C. P. Gommenginger, B. Jacob, and J. Staneva, "First multi-year assessment of Sentinel-1 radial velocity products using HF radar currents in a coastal environment," *Remote Sens. Environ.*, vol. 268, Jan. 2022, Art. no. 112758.

[19] F. Ardhuin et al., "Small-scale open ocean currents have large effects on wind wave heights," *J. Geophys. Res., Oceans*, vol. 122, no. 6, pp. 4500–4517, Jun. 2017.

[20] V. Kudryavtsev, M. Yurovskaya, B. Chapron, F. Collard, and C. Donlon, "Sun glitter imagery of surface waves. Part 2: Waves transformation on ocean currents," *J. Geophys. Res., Oceans*, vol. 122, no. 2, pp. 1384–1399, Feb. 2017.

[21] L. C. Laurindo, A. J. Mariano, and R. Lumpkin, "An improved near-surface velocity climatology for the global ocean from drifter observations," *Deep Sea Res. I, Oceanographic Res. Papers*, vol. 124, pp. 73–92, Jun. 2017.

[22] W. Alpers and I. Hennings, "A theory of the imaging mechanism of underwater bottom topography by real and synthetic aperture radar," *J. Geophys. Res.*, vol. 89, no. 6, pp. 10529–10546, 1984.

[23] D. E. Barrick, "HF radio oceanography—A review," *Boundary-Layer Meteorol.*, vol. 13, nos. 1–4, pp. 23–43, Jan. 1978.

[24] P. Lorente, J. Soto-Navarro, E. A. Fanjul, and S. Piedracoba, "Accuracy assessment of high frequency radar current measurements in the Strait of Gibraltar," *J. Oper. Oceanogr.*, vol. 7, no. 2, pp. 59–73, 2014.

[25] A. Kalampokis, M. Uttieri, P.-M. Poulain, and E. Zambianchi, "Validation of HF radar-derived currents in the Gulf of Naples with Lagrangian data," *IEEE Geosci. Remote Sens. Lett.*, vol. 13, no. 10, pp. 1452–1456, Oct. 2016.

[26] B. Emery and L. Washburn, "Uncertainty estimates for SeaSonde HF radar ocean current observations," *J. Atmos. Ocean. Technol.*, vol. 36, no. 2, pp. 231–247, 2019.

[27] J. B. Edson et al., "On the exchange of momentum over the open ocean," *J. Phys. Oceanogr.*, vol. 43, no. 8, pp. 1589–1610, 2013.

[28] A. Lygre and H. E. Krogstad, "Maximum entropy estimation of the directional distribution in ocean wave spectra," *J. Phys. Oceanogr.*, vol. 16, no. 12, pp. 2052–2060, Dec. 1986.

Shengren Fan received the B.S. degree in atmosphere sciences and the M.S. degree in marine meteorology from the Nanjing University of Information Science and Technology, Nanjing, China, in 2016 and 2019, respectively, where he is currently pursuing the Ph.D. degree in marine meteorology.

His research interests include microwave scattering numerical simulation, tropical cyclone remote sensing through dual-polarization synthetic aperture radar, and ocean current retrieved from SAR measurements.

Biao Zhang (Senior Member, IEEE) received the B.S. degree in surveying and mapping engineering from the China University of Petroleum, Dongying, China, in 2003, and the Ph.D. degree in physical oceanography from the Institute of Oceanology, Chinese Academy of Sciences, Qingdao, China, in 2008.

He was with the Bedford Institute of Oceanography, Dartmouth, NS, Canada, from 2008 to 2011, where he was a Post-Doctoral Fellow and was involved in developing synthetic aperture radar ocean surface wave and wind retrieval algorithms and products. He is currently a Professor with the School of Marine Sciences, Nanjing University of Information Science and Technology (NUIST), Nanjing, China. His research interests include satellite remote sensing of marine dynamic environments and tropical cyclones, air–sea interaction under extreme weather conditions, arctic sea ice monitoring by active and passive microwave sensors, and radar constellation mission.

Dr. Zhang was a recipient of the Visiting Fellow Scholarship of Natural Sciences and Engineering Research Council of Canada. He received the first award in Science and Technology from Jiangsu Province in 2017, the first award in Ocean Science and Technology from the State Oceanic Administration of China, and the second award in Natural Science from the Ministry of Education of China in 2014. He was a recipient of the Outstanding Young Scientist Award by National Science Foundation of China in 2016. He was selected as "Six Talent Peaks" of Jiangsu Province in 2018.

Artem Moiseev received the M.S. degree in oceanography from the Russian State Hydrometeorological University, St. Petersburg, Russia, in 2016, and the Ph.D. degree from the University of Bergen, Bergen, Norway, in 2021.

He is currently a researcher at Nansen Environmental and Remote Sensing Center, Bergen. He focuses on the development and utilization of the Doppler shift product from Sentinel-1A/B SAR.

Vladimir Kudryavtsev received the Ph.D. and Senior Doctorate degrees in geophysics/marine physics from the Marine Hydrophysical Institute (MHI), Sevastopol, Russia, in 1981 and 1991, respectively.

In 1976, he joined MHI. From 2005 to 2013, he was with the Nansen Center, St. Petersburg, Russia. Since 2002, he has been a Professor with the Russian State Hydrometeorological University, St. Petersburg, where he is currently the Head of the Satellite Oceanography Laboratory. He is also a part-time Principal Scientist with MHI, and until June 2016 also held a part-time Senior Position II with the Nansen Center, Bergen, Norway. His research interests include air–sea interaction, atmospheric and oceanic boundary layers, and radar and optical imaging of the ocean surface.

Johnny A. Johannessen received the Dr.Philos. degree from the University of Bergen, Bergen, Norway, in 1997.

He is currently an Acting Director with the Nansen Environmental and Remote Sensing Center, Bergen. He also holds an Adjunct Position at the Geophysical Institute, University of Bergen. He has 35 years' experience in satellite remote sensing in oceanography and sea ice research. In particular, he has focused on the use of satellite remote sensing to advance the understanding of mesoscale processes and air–sea-ice interaction associated with ocean fronts and eddies. He has also had central involvement in the development and implementation of the Marine Environmental Monitoring Service under the European Copernicus initiative. He has authored/coauthored more than 200 scientific and technical publications and reports of which 88 articles are published (or in press) in international peer-reviewed journals.

Bertrand Chapron was born in Paris, France, in 1962. He received the B.Eng. degree from the Institut National Polytechnique de Grenoble, Grenoble, France, in 1984, and the Doctorate National (Ph.D.) degree in fluid mechanics from the University of Aix-Marseille II, Marseille, France, in 1988.

He spent three years as a Post-Doctoral Research Associate at the NASA/GSFC/Wallops Flight Facility, Wallops Island, VA, USA. He has experience in applied mathematics, physical oceanography, electromagnetic waves theory, and its application to ocean remote sensing. He is currently responsible for the Oceanography from Space Laboratory, IFREMER, Plouzané, France.